

Capillary electrophoresis as a fragment screening tool to cross-validate hits from chromogenic assay: application to FXIIa

C. Davoine^{a,b}, M. Fillet^{b,†}, L. Pochet^{a,†,*}

^aNamur Medicine & Drug Innovation Center (NAME DIC – NARILIS), University of Namur, Rue de Bruxelles 61, 5000 Namur, Belgium

^bLaboratory for the Analysis of Medicines (LAM), Department of Pharmacy, CIRIM, University of Liege, Place du 20 Août 7, 4000 Liège, Belgium

[†] equally contributed to the work

*Corresponding author. E-mail address: lionel.pochet@unamur.be.

Postal address: Rue de Bruxelles 61, 5000 Namur, Belgium

Abstract

In this study, a partial-filling affinity capillary electrophoresis (pf-ACE) method was developed for the cross-validation of fragment hits revealed by chromogenic factor XIIa (FXIIa) assay. Chromogenic assay produces false positives, mainly due to spectrophotometric interferences and sample purity issues. pf-ACE was selected as counter-screening technology because of its separative character and the fact that the target does not have to be attached or tagged. The effects of protein plug length, applied voltage and composition of the running buffer were examined and optimized. Detection limit in terms of dissociation constant was estimated at 400 μM . The affinity evaluation was performed close to physiological conditions (pH 7.4, ionic strength 0.13 mol L⁻¹) in a poly(ethylene oxide)-coated capillary of 75 μm internal diameter x 33 cm length with an applied voltage of 3 kV. This method uncovered chromogenic assay's false positives due to zinc contamination. Moreover, pf-ACE supported the evaluation of compounds absorbing at 405 nm.

Keywords

Fragment-based lead discovery; serine proteinase inhibitors; capillary electrophoresis; chromogenic assay; factor XIIa; false positive.

Abbreviations

ACE, affinity capillary electrophoresis; BZM, benzamidine; FXII(a), (activated) coagulation factor XII; FBLD, fragment-based lead discovery; μ_A , electrophoretic mobility of the free analyte; $\mu_{A,eff}$, effective electrophoretic mobility inside the target plug; μ_{Cpl} , electrophoretic mobility of the complex analyte-target; μ_{obs} , observed electrophoretic mobility of the analyte in the presence of the target; ms-ACE, mobility-shift affinity capillary electrophoresis; PABZM, para-aminobenzamidine; pf-ACE, partial-filling affinity capillary electrophoresis; PhGu, phenylguanidine.

Introduction

Coagulation factor XIIa (FXIIa) is a S1A serine protease implicated in several physiological pathways including the intrinsic coagulation pathway, the kallikrein-kinin system, and the immune response [1,2]. Monoclonal antibodies at phase II clinical stage are evaluated in artificial surface-induced thrombosis [3], coronavirus disease [4], and hereditary angioedema [5]. FXIIa inhibitors could target a primary cause of such thrombosis without increasing bleeding risk and with additional anti-inflammatory properties [6,7]. Two inherited inflammatory pathologies, namely type III hereditary angioedema [8] and FXII-associated cold autoinflammatory syndrome [9], are associated with a FXII mutation which increases its susceptibility to activation. FXII is also an emerging research field in neuroinflammatory disorders since recent studies highlight its role in Alzheimer's disease and multiple sclerosis [10–13]. The FXII/FXIIa inhibitors currently under development include peptides, proteins, antibodies, and RNA-based technologies [14]. In contrast, only a few data regarding the design of selective small molecular-weight inhibitors of FXIIa are available [15–19]. Among these, our laboratory previously developed 3-carboxamido-benzopyrans [15–17]. For further developments, we decided to apply a fragment-based lead discovery approach (FBLD) to facilitate chemical exploration of FXIIa active site.

FBLD has become a widespread strategy applied in industries and academia to find innovative lead compounds [20]. The key concept in FBLD is that the exploration of the target chemical space is more efficient if small molecular weight compounds or fragments are used. Fragments are less likely to include motifs that impede binding. However, typical fragment equilibrium dissociation constants (K_D) are in the hundreds μ M to low mM range. Therefore, for a successful FBLD program, the fragment screening method needs to detect and gauge such weak affinity [21]. Biochemical assays and ligand-based NMR are the most popular approaches [20]. Biochemical assays require a low amount of protein, are high throughput and straightforward to establish. But they are burdened with various interferences such as aggregators, fluorescent compounds or impurities [21–23]. Ligand-based NMR is a powerful method that can detect binding at fragment concentration around or below its K_D . NMR can also give some structural information. The main limitation is the large amount of protein required [21]. Other biophysical techniques, such as surface plasmon resonance, thermal shift analysis, and X-ray crystallography, are also commonly used in FBLD screening [20,21]. Strengths and limitations of these biophysical methods in drug discovery are reviewed elsewhere [24]. Since the primary screening of our FXIIa FBLD program is a chromogenic assay, the development of a separative method as counter-screen was necessary to avoid wasting synthetic efforts on false positives.

Affinity capillary electrophoresis (ACE) is an emerging microfluidic screening technology based on the modification of the charge-to-size ratio of an analyte upon interaction with the target [25,26]. Similarly to weak affinity chromatography, a shift in analyte migration time is observed if a binding event occurs between the analyte and the target loaded in the capillary. ACE has the advantages of not requiring highly pure analyte nor target modification [26]. An increasing number of examples are described in the literature [27–31]. ACE is a general term that refers to various system configurations [25,32]. Among these, the most common is the so-called mobility-shift ACE (ms-ACE). For ms-ACE analysis, the capillary is pre-filled with a target-spiked buffer and a small amount of analyte is injected at one end of the capillary. When the voltage is applied, the analyte migrates through this target solution and, upon

binding, a shift in migration time is observed [26]. This shift is linked to a modification of the electrophoretic mobility of the analyte. In the case of fast equilibrium, a steady-state that depends on the target concentration and the binding constant occurs between free analyte and analyte-target complex. Therefore, the electrophoretic mobility of the analyte in the target-spiked buffer is a concentration-weighted average of the free analyte mobility (μ_A – unbound fraction) and the mobility of the complex (μ_{Cpl} – bound fraction) [25,33]. But ms-ACE is highly target-consuming because the vials that are at each end of the capillary during analysis need to be filled with the target-spiked buffer. This requirement leads to a consumption of more than 100 μL of the target-spiked buffer for each run. To lower target consumption and to avoid its presence during UV detection, we selected a variant of ms-ACE, known as partial-filling ACE (pf-ACE). In pf-ACE, only a part of the capillary, called the target plug, is pre-filled with the target-containing buffer. The rest of the capillary is filled with pure buffer. When the voltage is applied, the analyte migrates through the target plug and reaches the detector in the target-free buffer. Because the capillary is partially filled with the target, the observed analyte mobility (μ_{obs}) is a combination of the effective analyte mobility inside the plug ($\mu_{A,eff}$) and μ_A , as shown in Figure 1. In consequence, to observe a shift in the μ_{obs} (and thus in the analyte migration time), μ_{Cpl} has to be significantly different from μ_A [25,34].

This paper describes the development and the evaluation of a pf-ACE method with FXIIa as target for fragment counter-screen. The developed pf-ACE method was applied to the screening of a small focused library and the results were compared to those obtained with the chromogenic assay. Moreover, the impact of low-level metallic contamination on the two methods was also investigated and discussed.

Materials and methods

1. Chemicals and reagents

Benzamidine (BZM), pentamidine isethionate, 4-aminomethyl benzamidine dihydrochloride (compound 11), 3-aminomethyl benzamidine dihydrochloride (compound 12), 3-chlorobenzamidine hydrochloride (compound 5), 3,5-difluorobenzamidine hydrochloride (compound 17), diminazene aceturate (compound 4), Trizma® hydrochloride (Tris-HCl), poly(ethylene oxide) (PEO) (average M_v 200,000), 4-(2-Hydroxyethyl)piperazine-1-ethanesulfonic acid (HEPES), HEPES sodium salt (HEPES-Na), zinc sulfate heptahydrate (ZnSO_4), copper sulfate (CuSO_4), Tween® 20, Triton™ X-100, nafamostat mesylate, palladium(II) bromide, nickel(II) sulfate hexahydrate, iron(II) sulfate heptahydrate, iron(III) chloride hexahydrate, barium nitrate, calcium carbonate, magnesium sulfate heptahydrate, manganese(II) sulfate monohydrate, lead(II) nitrate, and cobalt(II) nitrate hexahydrate were sourced from Sigma-Aldrich (Saint-Louis, MO, USA). Para-aminobenzamidine (PABZM), phenylguanidine (PhGu), 1-benzothiophene-3-carboximidamide hydrochloride (compound 21), 2-methyl-1,3-thiazole-4-carboximidamide hydrochloride (compound 22), 3-furancarboximidamide hydrochloride (compound 23), nitric acid, HPLC-grade ethanol, trans-1,2-Diaminocyclohexane-N,N,N',N'-tetraacetic acid monohydrate (CDTA), N,N-dimethylformamide (DMF), formic acid, trifluoroacetic acid, and HPLC-grade acetonitrile were acquired from Acros Organics (New Jersey, USA). 6-amidino-2-naphthol methanesulfonate (compound 10), 4-hydroxybenzamidine hydrochloride (compound 13), pyridine-3-carboximidamide monohydrochloride (compound 9), and 4-amidinobenzamide hydrochloride

(compound 14) were provided by TCI Europe (Zwijndrecht, Belgium). Ortho-phosphoric acid 85% (H₃PO₄), sodium acetate (Acetate-Na), sodium chloride (NaCl), hydrochloric acid fuming 37% (HCl), sodium tetraborate decahydrate and sodium dodecyl sulfate were obtained from Merck (Darmstadt, Germany). Sodium hydroxide (NaOH) and dimethyl sulfoxide (DMSO) were provided from VWR (Leuven, Belgium). The substrate S-2302 was purchased from Werfen (Breda, Netherlands). Fragments Z234894731 (compound 1), Z1211228967 (compound 20), Z1263820361 (compound 3), Z234895267 (compound 2), Z839575938 (compound 15), Z2146514452 (compound 7), Z1295543851 (compound 24), Z199055442 (compound 16), Z3230795493 (compound 6), Z2895180539 (compound 19), Z1258943398 (compound 8), and Z2310699378 (compound 18) were acquired from Enamine (New Jersey, USA). Human plasma β -FXIIa was purchased from Molecular Innovations (Novi, MI), and was supplied as a 1.12mg/mL solution. The buffer consists of 4mM Acetate-Na, 0.15M NaCl at pH 5.3. Reported purity was > 95% by SDS-PAGE. Ultrapure water was produced by a Milli-Q equipment (Millipore, Bedford, MA, USA) and the Chromafil® Xtra PVDF syringe filters (0.2 μ m) were obtained from Macherey-Nagel (Duren, Germany). The physico-chemical properties of the fragment library, such as aqueous solubility and global charge at pH 7.4, were computed by MarvinSketch 19.27 (ChemAxon Ltd., Budapest, Hungary).

2. Samples stock solutions

Stock solutions of the tested molecules were prepared at 50 mM in DMSO and stored at -80°C, protected from light. To prepare the contaminated reference compounds, the mass of reference compound to obtain a stock solution of 50 mM was calculated and 5% of the mass was replaced by Zn²⁺ or Cu²⁺.

3. Virtual high throughput screening

Schrödinger Maestro 2019-2 software package (LLC, New York, NY) was used for the structure-based virtual screening. A virtual library of 2858 referenced drugs was optimized and energetically minimized via OPLS3 force field algorithm implemented in the LigPrep module of Schrödinger suite. The Epik tool was used to predict the ionization states of the ligands at pH 7 \pm 2 and to generate tautomers. Salts were then removed and all stereoisomers were generated. The prepared 3D structures were saved as maestro format. X-ray crystal structure of β -FXIIa complexed with BZM (PDB ID: 6B74) [35] was imported from RCSB Protein Data Bank (<http://www.rcsb.org/>). PrepWiz module included in Schrödinger suite performed the protein preparation of 6B74. The protein was first preprocessed to assign the bond orders. Water molecules implicated in less than three H bonds with the protein were deleted. The ligands were docked using GLIDE v8.3 docking with standard precision (SP) mode.

4. Chromogenic FXIIa assay

4.1. Instrumentation

All activity assays were performed on a multi-mode microplate reader SpectraMax iD3 (Molecular Devices, San Jose, CA, USA) operated by SoftMax Pro version 7.0.3 (Molecular Devices, San Jose, CA, USA). The instrument is equipped with plate shaking, injectors and temperature control system (5°C above the ambient temperature to 66°C \pm 1.0°C). Transparent 96-well flat-bottom polystyrene NBS microplate (Product No. 3641) were provided by Corning (New York, USA).

4.2. Procedure

Stock solutions of the tested compounds were diluted at 33.33 mM with DMSO. The kinetic buffer was made up of 30 mM HEPES, 150 mM NaCl and 0.005% Triton-X-100, adjusted at pH 7.4 with 1 M NaOH. 6 μ L of tested compound in DMSO (or DMSO alone), 10 μ L of human β -FXIIa (290 nM), and 164 μ L of the kinetic buffer are mixed for 5 sec and incubated for 10 min at 37°C. 20 μ L of 2.5 mM S-2302 are then injected in each well to start the reaction. The release of para-nitroaniline is recorded for 3.5 minutes at 405 nm. Between each absorbance read, the plate is shaken for 1 sec. For the determination of inhibition constant (K_i), the concentration of S-2302 injected was varied (54.7 μ M, 109.4 μ M, 218.8 μ M, 437.5 μ M, 875 μ M, 1.75 mM, 3.5 mM, and 7 mM).

4.3. Data analysis

For the treatment of activity data generated during screening, SoftMax Pro 7.0.3 (Molecular Devices, San Jose, CA, USA) was used to extract the slope of the kinetic reaction between 15 s and 200 s and to transform it in inhibition percentage by Equation 1.

$$\text{Inhibition (\%)} = \left(1 - \frac{v_i}{v_0}\right) \cdot 100 \quad (\text{Eq. 1})$$

where v_i and v_0 are the slope of the kinetic reaction with an inhibitor and with the vehicle alone, respectively.

To determine the inhibitory potency (IC_{50}), the 4-parameters logistic curve fit algorithm of SoftMax Pro 7.0.3 (Molecular Devices, San Jose, CA, USA) was forced in a 2-parameters logistic (Equation 2) by fixing the two horizontal asymptotes at 0% and 100% inhibition, as recommended by Copeland [36].

$$\text{Inhibition (\%)} = \left(1 - \frac{1}{1 + \left(\frac{[I]}{IC_{50}}\right)^h}\right) \cdot 100 \quad (\text{Eq. 2})$$

where [I] is the concentration of the inhibitor and h is the Hill slope.

The analysis of kinetic data for the determination of K_i was performed using the program DynaFit version 4.08.148 [37]. The initial reaction rates were determined by non-linear regression on the progress curves using the hybrid Trust-Region algorithm. To determine K_i , the initial reaction rates were then fitted to four inhibition mechanisms (competitive, uncompetitive, noncompetitive and mixed) under rapid-equilibrium approximation using the hybrid Trust-Region algorithm. Statistical model discrimination analysis was performed using the Bayesian Information Criterion (BIC) and the Akaike Information Criterion (AIC) to select the inhibition mechanism.

5. Partial-filling affinity capillary electrophoresis (pf-ACE) method

5.1. Instrumentation

All CE experiments were performed on a Hewlett Packard ^{3D}Capillary Electrophoresis system (Agilent Technologies, Waldbronn, Germany) operated by Agilent OpenLab CDS C.01.07 (27) software. The instrument was equipped with an autosampler, an on-capillary DAD and a temperature control system (15-60°C \pm 0.1°C). Bare-fused silica capillaries (75 μ m I.D., 375 μ m O.D.) were provided by Polymicro Technologies (Phoenix, AZ, USA). In the optimal conditions, the effective and the total lengths of the capillary were 24.5 cm and 33 cm, respectively. During analysis, the capillary cassette was thermostated at 25°C by high-velocity air stream.

5.2. Coating procedure and rinsing procedure

The capillary was PEO-coated according to Farças et al.[27]. Briefly, new capillaries were rinsed by successive flushes with H₂O, 1 M NaOH, 0.1 M NaOH, and H₂O (5 min each). The coating was then applied by flushing successively with H₂O (5 min), 1 M NaOH (5 min), 1 M HCl (10 min), H₂O (10 min), 0.2% PEO (5 min), and H₂O (5 min). Each day, the dynamic coating was regenerated by successive flushes of H₂O (5 min), 1 M HCl (5 min), 0.2% PEO (5 min). Before each run, the coating was also regenerated by flushing H₂O (3 min), 1 M HCl (3 min), 0.2% PEO (5 min), and background electrolyte (BGE) (2 min). After each run with β-FXIIa, a pressure of -100 mbar was applied at the inlet during 2 min, followed by a flush of BGE (2 min). After 6 runs with β-FXIIa, the 2 M HCl rinsing procedure reported by Suratman et al. [38] was performed. After each run without β-FXIIa, the capillary was flushed with BGE during 2 min. Flushes correspond to the application of approximately 1 bar at the inlet vial. The 0.2% PEO solution was prepared in water containing 0.1 M HCl.

5.3. Preparation of buffers and samples

The final BGE was composed of an acetate buffer (4 mM acetate sodium, 150 mM NaCl, adjusted at pH 5.3 with 0.1 M H₃PO₄) and a Tris-HEPES buffer (10 mM Tris HCl, 10 mM HEPES-Na, 100 mM NaCl, adjusted at pH 7.4 with 0.1 M H₃PO₄) in 1:2 (v/v). Before the experiment, the stock solutions were diluted with BGE to obtain an approximative concentration of 75 μM, followed by a 10-fold dilution with H₂O (7.5 μM final concentration). The stock solution of β-FXIIa (37.44 μM in the acetate buffer) was 3-fold diluted with the Tris-HEPES buffer containing 0.05% Tween 20 to reach the final concentration of 12.5 μM.

5.4. Determination of complex dissociation constant

The selected ligands were kept at 7.5 μM, while the β-FXIIa plug length was varied (0, 3.6, 6.4, 13.7, and 19.6 cm). 12.5 μM β-FXIIa was first injected hydrodynamically at 80 mbar for 0, 8, 14, 30, or 43 sec. Then the ligand was injected at 20 mbar for 5 sec, followed by a short plug of BGE (injected at 20 mbar for 3 sec). The applied voltage was set at 3 kV. PABZM and pentamidine were detected at 290 nm and 260 nm, respectively. Each condition was done in duplicate. The complex dissociation constant (K_D) of PABZM and pentamidine were determined according to Equation 3 reported by Nilsson et al. [39]:

$$\frac{1}{K_D} = \frac{\pi \cdot r^2 \cdot l_{det}}{M_{t0,det}} \cdot \frac{d\Delta M_t}{dn} \text{ where } n = c \cdot \pi \cdot r^2 \cdot l_{plug} \text{ (Eq. 3)}$$

where r is the inner radius of the capillary (dm), $M_{t0,det}$ is the migration time of the ligand in pure BGE (min), ΔM_t is the difference in migration time of the ligand with and without loaded protein (min), n is the amount of protein (mol), l_{det} is the effective length of the capillary (dm) and l_{plug} is the plug length (dm).

The l_{plug} is calculated by the Equation 4:

$$l_{plug} = l_{det} \cdot \frac{t_{plug}}{t_{det}} \text{ (Eq. 4)}$$

where l_{plug} , l_{det} , t_{plug} , and t_{det} are the plug length (dm), the effective length (dm), the protein injection time (min), and the time to reach the detector (min), respectively.

The time to reach the detector was determined by measuring the time necessary to observe a jump in absorbance after the application of 80 mbar to a vial containing 12.5 μM of β-FXIIa.

5.5. Conditions for library screening

12.5 μM $\beta\text{-FXIIa}$ was first hydrodynamically injected at 80 mbar for 0 or 43 sec. Then the screened compound was injected at 20 mbar for 5 sec, followed by a short plug of BGE (injected at 20 mbar for 3 sec). The mobility of the analyte (μ_A) was determined in the capillary only filled with BGE. In partial-filling, the mobility observed in the capillary partially filled with $\beta\text{-FXIIa}$ (μ_{obs}) is not equal to the effective mobility inside the $\beta\text{-FXIIa}$ plug ($\mu_{A,\text{eff}}$). Based on the following Equation 5 described by Ansorge et al. [34], $\mu_{A,\text{eff}}$ was calculated considering that the EOF is equal to zero (due to the PEO coating).

$$\mu_{\text{obs}} = \frac{(\mu_A + \mu_{\text{EOF}}) \cdot (\mu_{A,\text{eff}} + \mu_{\text{EOF}} - \mu_B)}{(\mu_{A,\text{eff}} + \mu_{\text{EOF}} - \mu_B) + x \cdot (\mu_A - \mu_{A,\text{eff}})} \text{ where } \mu_B = \mu_L + \mu_{\text{EOF}} \quad (\text{Eq. 5})$$

If $\mu_{\text{EOF}} = 0$, $\mu_B = \mu_L$ and the equation becomes:

$$\mu_{\text{obs}} = \frac{\mu_A \cdot (\mu_{A,\text{eff}} - \mu_L)}{(\mu_{A,\text{eff}} - \mu_L) + x \cdot (\mu_A - \mu_{A,\text{eff}})} \quad (\text{Eq. 6})$$

After rearrangement:

$$\mu_{A,\text{eff}} = \frac{\mu_{\text{obs}} \cdot \mu_L - \mu_A \cdot (x \cdot \mu_{\text{obs}} + \mu_L)}{(1-x) \cdot \mu_{\text{obs}} - \mu_A} \quad (\text{Eq. 7})$$

Bound fraction (% - Equation 8) was then used to rank the fragments. Because we were working with proteins and small molecules, the mobility of the complex (μ_{cpl}) can be approximated by the mobility of the protein alone (μ_L).

$$\text{Bound fraction (\%)} = \frac{(\mu_{A,\text{eff}} - \mu_A)}{(\mu_{\text{cpl}} - \mu_A)} \cdot 100\% \quad \text{where } \mu_{\text{cpl}} = \mu_L \quad (\text{Eq. 8})$$

To determine μ_L , 12.5 μM $\beta\text{-FXIIa}$ was hydrodynamically injected at the outlet by applying -20 mbar at the inlet vial for 5 sec, followed by a short plug of BGE (injected at -20 mbar for 3 sec). The applied voltage was set at 3 kV. $\beta\text{-FXIIa}$ was detected at 230 nm.

5.6. Data treatment

The migration time were determined by CEVal software version 0.6h7 [40] using the Haarhoof Van der Linde fit to take into account peak distortion. The electrophoretic mobilities (in $10^{-9} \cdot \text{m}^2 \cdot \text{V}^{-1} \cdot \text{s}^{-1}$) were then calculated by applying Equation 9:

$$\mu = \frac{(L_{\text{tot}} - L_{\text{eff}})}{V \cdot M_t} \cdot 10^9 \quad (\text{Eq. 9})$$

where L_{tot} and L_{eff} are the total and effective length of the capillary in m, V is the voltage applied in V and M_t is the migration time in sec.

Linear regression for the determination of complex dissociation constant (K_D) and statistical analysis were made with Microsoft Office Excel 2016 (Microsoft, Redmond, WA, USA).

Regarding error propagation, the general Equation 10 was used:

$$\sigma_{\bar{f}} = \sqrt{\sum_{i=1}^n \left(\frac{\partial f}{\partial x_i} \right)^2 \sigma_{x_i}^2} \quad (\text{Eq. 10})$$

6. Identification of the metallic contaminant by CE

The identification of the metallic contaminant was performed using a bare-fused silica capillary of 50 μm I.D. (Polymicro Technologies, Phoenix, AZ, USA). The effective and the total lengths of the capillary were 40 cm and 48.5 cm, respectively. During analysis, the capillary cassette was thermostated at 25°C by high-velocity air stream. The BGE consists of 10.8 mM sodium borate, 5 mM CDTA, 10% ethanol (adjusted at pH 9 with 1 M NaOH). Each day, the capillary was rinsed by successive flushes of 1 M NaOH, H₂O, and BGE (10 min each). Before each run, the capillary was preconditioned by flushing BGE with 25 mM

sodium dodecyl sulfate and BGE (3 min each). Samples were first dissolved in a mineralization solvent (65% nitric acid: 5 M HCl; 20:80) and then 50-fold diluted with the dissolution solvent (0.05% DMF, 7 mM CDTA in water adjusted at pH 4 with 2 M HCl). For the selectivity profiling, the twelve metal elements were injected at 3 mM concentration. For spiked samples, 1.5 mM of Zn^{2+} were added. Samples were hydrodynamically injected in the capillary at 20 mbar for 5 sec, followed by a short plug of BGE (injected at 20 mbar for 3 sec). The applied voltage was set at 20 kV. Metals were detected at 200 nm with 550 nm as reference wavelength.

Results and discussion

1. Implementation of reference compounds

To develop the pf-ACE method as a fragment screening methodology, reference compounds with fast equilibrium were needed across the μM -mM range of affinity. For FXIIa, this type of molecules is poorly described in the literature. Only the inhibition constant (K_i) of BZM was previously reported (BZM K_i on β -FXIIa = 1.12 mM at pH 7.2) [41]. This fragment was also crystallized in the active site of FXIIa (PDB ID: 6B74) [35]. A similar serine protease inhibitor is p-aminobenzamidine (PABZM) but its K_i on β -FXIIa was not previously reported. We thus determined the K_i of PABZM by chromogenic assay (see section 4, Table 1, and Figure S1A) (PABZM K_i on β -FXIIa = $163.2 \pm 0.5 \mu\text{M}$ with a competitive behavior). In our previous coumarin series, phenylguanidine (PhGu) was highlighted as a key feature [17]. This fragment was evaluated and exhibits a very weak affinity (see Table 1). Overall, a compound with a low μM affinity was still missing. Nafamostat was first considered. Nevertheless, a non-ideal kinetic behavior was suspected based on mechanistic studies performed on bovine pancreatic trypsin [42]. The slow reversibility of nafamostat on FXIIa was confirmed by jump-dilution experiment (see Figure S2). Without potent compound with an adequate behavior, we decided to carry out a virtual high throughput screening on referenced drugs. Among them, pentamidine obtained the best docking score (-10.883). Its K_i was determined at $12.4 \pm 0.1 \mu\text{M}$ with a competitive behavior (see Table 1 and Figure S1B).

2. Initial ACE method selection

To minimize exosite binding [43] and protein-silica wall interactions, we decided to work with the β form of FXIIa. β -FXIIa is a physiological form of FXIIa which lost the non-catalytic domains found in α -FXIIa, including those required for the binding to negatively-charged surfaces [1,44]. Some of these non-catalytic domains carry continuous patches of positively charged residues which could entail α -FXIIa adsorption to silica by Coulomb interactions with SiO^- [44,45]. These functional patches are not present in β -FXIIa [1].

As an objective, we established that the CE method needs to discriminate PABZM from BZM in terms of bound fraction. In our medicinal chemistry program, we are searching for fragments with higher affinity than the already known BZM. We started with a previously developed method for thrombin [27], but the direct transposition of the method was not achievable. First, the 25 μM target concentration cannot be reached for practical reasons. Secondly, FXIIa is a negatively-charged protein [46] in the operating conditions, as confirmed by its migration measured by CE. Therefore, the mathematical model used for effective

mobility calculation was modified according to Ansorge et al. [34] to integrate the charge of the target (see Materials and Methods).

3. pf-ACE method optimization

3.1. Sample injection and stacking

In experiment ran without target, the initial method showed large sample peaks with low intensity, inducing detectability issues with low UV-absorbing compounds. We also observed lack of repeatability in the applied pressure during injection. As described by Nilsson et al. [39], we investigated a longer injection time as well as sample stacking and inserted a short plug of BGE after the sample plug to prevent diffusion back to the anode. Each condition was made in triplicate with PABZM as analyte (see Table 2A). The RSDs of the migration times were similar for the tested conditions. The procedure with the longer injection time and the sample stacking provided better results with RSD value of 0.5% for AUC and was selected for further developments.

3.2. Protein plug length and rinsing procedure

With a target plug length of 5 cm, the calculated bound fractions were significantly different between pentamidine and PABZM but not between PABZM and BZM, leading to a limit of detection in affinity between 10 and 100 μ M approximately. Under the condition that the mobility of the complex is equal to the mobility of the target alone, the effective mobility becomes a function of the total target load only (in moles) [34,39]. This assumption can be assumed with small molecules and big targets like proteins [34]. To improve discrimination without increasing target concentration, we varied the protein plug length. In the initial configuration (capillary 75 μ m x 48.5 cm total length with injection at the short-end), the protein plug length could not be extended. Using a capillary of 33 cm total length (24.5 cm effective length) instead of 48.5 cm (40 cm effective length), we could expand 4-fold times the target plug length (20 cm instead of 5 cm), allowing the discrimination of PABZM from BZM. Moreover, rinsing procedures were reinvestigated [38,47]. Sodium hydroxide was excluded because it removed the PEO-coating and 2 M hydrochloric acid provided the best results (see Table 2B). Finally, 0.05% Tween® 20 was also added in the protein dilution buffer (10 mM Tris HCl, 10 mM HEPES-Na, 100 mM NaCl, pH 7.4) in order to minimize protein aggregation [48]. Altogether, the electrophoretic mobility of 56 controls during 7 days, performed in-between 21 runs with FXIIa, showed RSD of 1.8% (see Table 2B).

3.3. Buffer composition and applied voltage

The composition of the BGE was also adjusted. Polyethylene glycol 6000 was removed because it was reported that high molecular weight polyethylene glycol interacts with protein in aqueous solution and induces conformational changes [49]. Moreover, we also observed that longer plug length generated higher current at the same voltage. This observation suggested an inhomogeneous conductivity between the FXIIa plug and the BGE. Using the PeakMaster 6.0f8 program [50], computed conductivity of the FXIIa plug buffer and the BGE were estimated at 1.333 S/m and 1.202 S/m, respectively. This result supported that the buffer of the commercial FXIIa solution (4 mM acetate sodium, 150 mM NaCl, pH 5.3) has a significant impact on FXIIa plug conductivity. To mimic as closely as possible the composition of the FXIIa plug, the sodium acetate buffer was mixed with the previous BGE (10 mM Tris HCl, 10 mM HEPES-Na, 100 mM NaCl, pH 7.4) in the same proportion (acetate

buffer:Tris-HEPES buffer 1:2). The final BGE was then composed of 1.33 mM sodium acetate, 6.67 mM Trizma® hydrochloride, 6.67 mM HEPES sodium salt, and 117 mM sodium chloride. Its pH was measured at 7.4. With this modification, similar currents were generated within the different plug lengths. However, because of the increase in BGE conductivity, we had to check if the heat dissipation was still adequate by performing an Ohm's law plot. The current increased linearly between 0 and 3 kV, indicating an adequate heat dissipation in this range (see Figure S3). The slopes of the linear regression between 0-2.5 kV and 0-3 kV are, respectively, 18.4 and 18.4 while the slopes between 0-3.2 kV, 0-3.5 kV, and 0-4 kV are, respectively, 18.6, 18.7 and 19.0. Therefore, to avoid excessive Joule heating, the applied voltage was set at 3 kV, the latest point that do not increase the slope.

4. Determination of complex dissociation constant by pf-ACE

It could be observed that the binding of pentamidine leads to a peak broadening (Figure 2). In ACE, it is common that electromigration dispersion (EMD) is generated by the binding of the analyte to the target [51–53]. Indeed, we observed an increase in the peak width with the target plug length. At a virtually infinite target concentration, the analyte is fully bound to the target, no matter the analyte concentration [52]. At lower target concentration, the bound fraction of the analyte depends on its concentration in the sample zone. The dependance of the analyte concentration on its local bound fraction is strong when the analyte possess an high affinity for the target and when the ratio target/analyte is low [52,53]. As illustrated in figure S4, the stronger the fragment binds, the broader the peak. Even if EMD distorts the peak, the effective electrophoretic mobility is not affected. However, the electrophoretic mobility cannot be assigned at the peak apex anymore [40,51,54]. EMD-distorted peaks are accurately described by the Haarhoff-Van der Linde function [51]. Therefore, to correct the bias in the migration induced by EMD, we systematically performed a peak fitting with this function and extract the a_1 parameter as migration time (see Materials and Methods and Figure S4) [40,51,54].

To confirm that our method follows interactions accurately, the K_D of PABZM and pentamidine were evaluated according to Nilsson et al. [39] (see Materials and Methods). As illustrated in Figure 2, the target plug length was varied and the shift in migration time increased linearly with the molar amount of FXIIa. K_D was determined from the slope of the linear regression. As shown in Figure 2 and in Figure S5, the K_D was measured at $149 \pm 14 \mu\text{M}$ for PABZM (competitive inhibitor with K_i measured at $163.2 \pm 0.5 \mu\text{M}$ by chromogenic assay) and $6.30 \pm 0.07 \mu\text{M}$ for pentamidine (competitive inhibitor with K_i measured at $12.4 \pm 0.1 \mu\text{M}$ by chromogenic assay). Dissociation constant K_D and inhibition constant K_i strongly depends on the assay conditions, such as temperature, ionic strength, pH, and concentration of aprotic solvent [36]. K_i is determined through inhibition kinetics, while K_D is determined through a more direct measure of the binding [55]. All these factors could contribute to the discrepancy among the values obtained with both methods.

5. Library screening

After establishing the reliability of our approach, a library of 24 fragments were screened by the chromogenic assay and the developed pf-ACE method. Figure 3 displays the screening results obtained. To rank fragments, calculated bound fraction and inhibition percentage were used for pf-ACE and the chromogenic assay, respectively (see Materials and Methods).

5.1. Threshold for activity and affinity determination

In pf-ACE, each fragment was tested with and without target the same day. During the screening, 121 controls, consisting of BZM migration time monitoring, were passed on three different capillaries and the RSD was below 1.6% (see Table 2C). Within the same day, the RSD of the controls was below 1.1% (see Table 2C). For chromogenic FXIIa assay, the RSD of the control inhibition percentage (125 μ M PABZM) was 10.3%. The thresholds were set at three-fold the intra-day RSD of ACE controls (threshold at 3.3% for pf-ACE) and at three-fold the RSD of control inhibition percentages (threshold at 30.9% for chromogenic assay). On this basis, the affinity (in K_D) and the activity (in K_i) required to obtain a significant signal was estimated approximately at 400 μ M for pf-ACE and 1 mM for chromogenic assay, respectively.

5.2. Comparison of pf-ACE and chromogenic assay screening

As illustrated by Figure 3, a good correlation was observed between pf-ACE and the chromogenic assay results. Major differences were noticed with the compounds 1, 2, and 3. They exhibit a high ranking in the chromogenic assay but are under or near the threshold in pf-ACE. It is also important to mention that compound 4 interferes with spectrophotometric detection in chromogenic FXIIa assay. At 1 mM, the yellow color of compound 4 saturates the spectrophotometric detector which masks the liberation of para-nitroaniline. When the liberation of para-nitroaniline cannot be accurately recorded among time, it is impossible to determine if an inhibition of its release effectively occurs. Therefore, compounds absorbing at 405 nm induce uninterpretable results in the chromogenic assay. On the other hand, pf-ACE was able to evaluate compound 4 thanks to the separation before the detection.

5.3. Identification of the contaminant which leads to false positives

To explain the discrepancy between some results, we hypothesized that low concentrations of divalent metallic cations could interfere with the chromogenic assay. Indeed, zinc was previously reported as a common contaminant of Roche screening compounds which leads to false positives in many assays [56] and as an inhibitor of FXIIa amidolytic activity [57]. The chromogenic assay and pf-ACE were challenged by introducing 5% (w/w) metallic impurity (Zn^{2+} and Cu^{2+}) in PABZM and PhGu samples. As can be seen in Table S1, the calculated bound fractions obtained by the pf-ACE method were unaffected by the metallic contamination. But the chromogenic FXIIa assay showed a large increase in their inhibition percentages, particularly for PhGu. The IC_{50} of PhGu was 34-fold decreased by the 5% (w/w) Zn^{2+} (see Figure S6). After confirmation that only the chromogenic assay is impaired, the inhibition percentage at 1 mM and the IC_{50} were reevaluated in the presence and absence of 1 mM EDTA. The inhibition percentages at 1 mM of compounds 1, 2, and 3 were reduced by 30.7%, 32.6%, and 53.0%, respectively. Figure 4 shows that the IC_{50} of compound 3 shifted with the addition of 1 mM EDTA while the IC_{50} of PABZM remained unaffected. The addition of 1 mM EDTA also unmasked steep Hill slopes in the IC_{50} of compounds 1 and 2 (see Figure S7 and S8). This results suggested a promiscuous inhibition [58]. The metal element was identified by capillary electrophoresis using pre-capillary CDTA complexation. Twelve metal elements were evaluated (see Figure S9). Four metal elements (Zn^{2+} , Pd^{2+} , Pb^{2+} , and Ni^{2+}) co-migrated but has distinctive UV spectra (see Figure S10). Based on electrophoretic mobility and UV spectrum of the peak observed in compounds 1-3, zinc contamination was suspected and then confirmed after spiking the samples with Zn^{2+} .

Indeed, in the three samples, the UV spectrum of the metallic contaminant was not modified (see Figure 5, S11 and S12).

5.4. Impurity profiling of the fragment library

Besides metallic contamination, reactive intermediates could also lead to misleading results in a fragment screen. If the screening is performed at 1 mM in chromogenic assay, a 1% impurity will reach a concentration of 10 μ M and could compromise the results in the chromogenic assay. To evaluate the number of compounds with potential purity issues in our small library, the samples were tested by UHPLC coupled to a mass spectrometer in scan mode as detector. 13 compounds of the 28 showed at least one additional peak beside the main peak (see Table S2). As highlighted with our small library, low-level impurities is a common FBLD pitfall and it is highly recommended to validate fragment hits with a orthogonal technique before engaging significant resources [23]. Thanks to its separative character, pf-ACE is less affected by sample contaminants and is suited for fragment cross-validation, as demonstrated by the detection of three false positives due to zinc contamination.

5.5. Medicinal chemistry perspective

Analyzing the screening results from a medicinal chemistry perspective afford some interesting insight around the BZM fragment. The best substitutions on the benzene ring were the introduction of chloride in meta position (compound 5) and amino in para position (PABZM). Modulations on the aromatic ring indicated that fused bicyclic aromatic rings are preferred. The three best aromatic rings were quinoline (compound 6), naphthalene (compound 7), and benzofuran (compound 8). Interestingly, the introduction of a nitrogen on the naphthalene ring next to the amidine has a positive effect (compound 6 compared to compound 7) while a loss of activity was observed with the substitution of the carbon in position 3 by a nitrogen on the benzene ring (compound 9 compared to BZM). The IC_{50} of compounds 6, 7, and 8 were, respectively, 298 (\pm 12) μ M, 633 (\pm 29) μ M, and 812 (\pm 40) μ M. A 2-fold improvement was observed when a hydroxy group is added in para position on compound 7 (compound 10 – IC_{50} = 387 \pm 10 μ M). Dicationic compounds, pentamidine and compound 4, were the most potent of the library. The IC_{50} of compound 4 is 114 (\pm 3) μ M.

6. Conclusion

Chromogenic assays are high throughput and straightforward to establish but they produce a significant number of false positives. The results presented in this paper demonstrate that the chromogenic FXIIa assay is sensitive to spectrophotometric interferences and the presence of a low-level metallic impurity. The zinc contamination led to three false positives. The evaluation of the fragments' purity showed that 46% of our library had at least one additional peak beside the main peak detected in UHPLC-MS. Very high purity is commonly not achieved and could generate misleading structure-activity relationships. Hence, cross-validation by orthogonal techniques is essential before starting synthetic efforts to avoid wasting time and resources. Our study showed that pf-ACE can be used for positively-charged fragment counter-screening. The technique is unaffected by metallic contamination and highly UV/Vis-absorbent compounds. Moreover, pf-ACE detects binding at fragment concentration below their K_D and only low μ M fragment concentration is necessary. Therefore, pf-ACE is less subject to solubility and aggregation issues. Although less sensitive

in our set-up, the separative character and the low fragment consumption make the pf-ACE method powerful for the cross-validation of fragment hits.

Declaration of competing interest

The authors declare no conflict of interest.

Acknowledgements

This work was supported by the Fonds National de la Recherche Scientifique – FNRS (Belgium) from which C. Davoine was a Research Fellow.

We gratefully acknowledge the contribution of the following colleagues: Alice Demelenne, Paul Emonts, and Marie-Jia Gou for their technical assistance and advices with the capillary electrophoresis instrument.

References

- [1] M. Didiasova, L. Wujak, L. Schaefer, M. Wygrecka, Factor XII in coagulation, inflammation and beyond, *Cell. Signal.* 51 (2018) 257–265. <https://doi.org/10.1016/j.cellsig.2018.08.006>.
- [2] N. Ziliotto, F. Bernardi, D. Jakimovski, R. Zivadinov, Coagulation Pathways in Neurological Diseases: Multiple Sclerosis, *Front. Neurol.* 10 (2019) 1–21. <https://doi.org/10.3389/fneur.2019.00409>.
- [3] Safety and Efficacy Study of AB023 (Xisomab 3G3) in End Stage Renal Disease Patients on Chronic Hemodialysis - Full Text View - ClinicalTrials.gov, (n.d.). <https://www.clinicaltrials.gov/ct2/show/study/NCT03612856?term=xisomab&draw=2&rank=2> (accessed August 12, 2020).
- [4] Treatment With CSL312 in Adults With Coronavirus Disease 2019 (COVID-19) - Full Text View - ClinicalTrials.gov, (n.d.). <https://www.clinicaltrials.gov/ct2/show/NCT04409509?term=csl312&draw=2&rank=3> (accessed September 3, 2020).
- [5] A Study to Investigate CSL312 in Subjects With Hereditary Angioedema (HAE) - Full Text View - ClinicalTrials.gov, (n.d.). <https://www.clinicaltrials.gov/ct2/show/NCT03712228?term=csl312&draw=2&rank=2> (accessed August 12, 2020).
- [6] N.C. Chan, J.I. Weitz, Antithrombotic Agents, *Circ. Res.* 124 (2019) 426–436. <https://doi.org/10.1161/CIRCRESAHA.118.313155>.
- [7] B. Tillman, D. Gailani, Inhibition of Factors XI and XII for Prevention of Thrombosis Induced by Artificial Surfaces, *Semin. Thromb. Hemost.* 44 (2018) 060–069. <https://doi.org/10.1055/s-0037-1603937>.
- [8] J. Björkqvist, S. de Maat, U. Lewandrowski, A. Di Gennaro, C. Oschatz, K. Schönig, M.M. Nöthen, C. Drouet, H. Braley, M.W. Nolte, A. Sickmann, C. Panousis, C. Maas, T. Renné, Defective glycosylation of coagulation factor XII underlies hereditary angioedema type III, *J. Clin. Invest.* 125 (2015) 3132–3146. <https://doi.org/10.1172/JCI77139>.
- [9] J. Scheffel, N.A. Mahnke, Z.L.M. Hofman, S. de Maat, J. Wu, H. Bonnekoh, R.J. Pengelly, S. Ennis, J.W. Holloway, M. Kirchner, P. Mertins, M.K. Church, M. Maurer, C. Maas, K. Krause, Cold-induced urticarial autoinflammatory syndrome related to factor XII activation, *Nat. Commun.* 11 (2020) 179. <https://doi.org/10.1038/s41467-019-13984-8>.
- [10] A.H. Schmaier, E.X. Stavrou, Factor XII - What's important but not commonly thought about, *Res. Pract. Thromb. Haemost.* 3 (2019) 599–606. <https://doi.org/10.1002/rth2.12235>.
- [11] H. Weidmann, L. Heikaus, A.T. Long, C. Naudin, H. Schlüter, T. Renné, The plasma contact system, a protease cascade at the nexus of inflammation, coagulation and

- immunity, *Biochim. Biophys. Acta - Mol. Cell Res.* 1864 (2017) 2118–2127. <https://doi.org/10.1016/j.bbamcr.2017.07.009>.
- [12] K.F. Nickel, A.T. Long, T.A. Fuchs, L.M. Butler, T. Renné, Factor XII as a Therapeutic Target in Thromboembolic and Inflammatory Diseases, *Arterioscler. Thromb. Vasc. Biol.* 37 (2017) 13–20. <https://doi.org/10.1161/ATVBAHA.116.308595>.
- [13] S. Lorenzano, M. Inglese, T. Koudriavtseva, Editorial: Role of Coagulation Pathways in Neurological Diseases, *Front. Neurol.* 10 (2019) 1–3. <https://doi.org/10.3389/fneur.2019.00791>.
- [14] B.F. Tillman, A. Gruber, O.J.T. McCarty, D. Gailani, Plasma contact factors as therapeutic targets, *Blood Rev.* 32 (2018) 433–448. <https://doi.org/10.1016/j.blre.2018.04.001>.
- [15] S. Robert, C. Bertolla, B. Masereel, J.-M. Dogné, L. Pochet, Novel 3-Carboxamide-coumarins as Potent and Selective FXIIa Inhibitors, *J. Med. Chem.* 51 (2008) 3077–3080. <https://doi.org/10.1021/jm8002697>.
- [16] C. Bouckaert, S. Serra, G. Rondelet, E. Dolušić, J. Wouters, J.-M. Dogné, R. Frédérick, L. Pochet, Synthesis, evaluation and structure-activity relationship of new 3-carboxamide coumarins as FXIIa inhibitors, *Eur. J. Med. Chem.* 110 (2016) 181–194. <https://doi.org/10.1016/j.ejmech.2016.01.023>.
- [17] C. Bouckaert, S. Zhu, J.W.P. Govers-Riemslog, M. Depoorter, S.L. Diamond, L. Pochet, Discovery and assessment of water soluble coumarins as inhibitors of the coagulation contact pathway, *Thromb. Res.* 157 (2017) 126–133. <https://doi.org/10.1016/j.thromres.2017.07.015>.
- [18] J.J.F. Chen, D.P. Visco, Identifying novel factor XIIIa inhibitors with PCA-GA-SVM developed vHTS models, *Eur. J. Med. Chem.* 140 (2017) 31–41. <https://doi.org/10.1016/j.ejmech.2017.08.056>.
- [19] H. Philippou, R. Foster, C. Fishwick, C. Reville, I. Yule, R. Taylor, A. Naylor, P.S. Fallon, S. Crosby, A. Hopkins, M.R. Stewart, N.L. Winfield, FACTOR XIIIa INHIBITORS, WO/2019/211585, 2019.
- [20] D.A. Erlanson, I.J.P. de Esch, W. Jahnke, C.N. Johnson, P.N. Mortenson, Fragment-to-Lead Medicinal Chemistry Publications in 2018, *J. Med. Chem.* (2020). <https://doi.org/10.1021/acs.jmedchem.9b01581>.
- [21] B. Lamoree, R.E. Hubbard, Current perspectives in fragment-based lead discovery (FBLD), *Essays Biochem.* 61 (2017) 453–464. <https://doi.org/10.1042/EBC20170028>.
- [22] G.M. Keseru, D.A. Erlanson, G.G. Ferenczy, M.M. Hann, C.W. Murray, S.D. Pickett, Design Principles for Fragment Libraries: Maximizing the Value of Learnings from Pharma Fragment-Based Drug Discovery (FBDD) Programs for Use in Academia, *J. Med. Chem.* 59 (2016) 8189–8206. <https://doi.org/10.1021/acs.jmedchem.6b00197>.
- [23] B.J. Davis, D.A. Erlanson, Learning from our mistakes : The ‘ unknown knowns ’ in fragment screening, *Bioorg. Med. Chem. Lett.* 23 (2013) 2844–2852. <https://doi.org/10.1016/j.bmcl.2013.03.028>.
- [24] J. Renaud, C. Chung, U.H. Danielson, U. Egner, M. Hennig, R.E. Hubbard, H. Nar, Biophysics in drug discovery: impact, challenges and opportunities, *Nat. Rev. Drug Discov.* (2016) 1–20. <https://doi.org/10.1038/nrd.2016.123>.
- [25] M. Olabi, M. Stein, H. Wätzig, Affinity capillary electrophoresis for studying interactions in life sciences, *Methods.* 146 (2018) 76–92. <https://doi.org/10.1016/j.ymeth.2018.05.006>.
- [26] E. Farcas, L. Pochet, J. Crommen, A. Servais, M. Fillet, Capillary electrophoresis in the context of drug discovery, *J. Pharm. Biomed. Anal.* 144 (2017) 195–212. <https://doi.org/10.1016/j.jpba.2017.02.022>.
- [27] E. Farcaş, C. Bouckaert, A.C. Servais, J. Hanson, L. Pochet, M. Fillet, Partial filling affinity capillary electrophoresis as a useful tool for fragment-based drug discovery: A proof of concept on thrombin, *Anal. Chim. Acta.* 984 (2017) 211–222. <https://doi.org/10.1016/j.aca.2017.06.035>.
- [28] I.O. Neaga, S. Hambye, E. Bodoki, C. Palmieri, E. Ansseau, A. Belayew, R. Oprean, B. Blankert, Affinity capillary electrophoresis for identification of active drug candidates

- in myotonic dystrophy type 1, *Anal. Bioanal. Chem.* 410 (2018) 4495–4507. <https://doi.org/10.1007/s00216-018-1107-6>.
- [29] M. Xu, C. Liu, M. Zhou, Q. Li, R. Wang, J. Kang, Screening of small-molecule inhibitors of protein-protein interaction with capillary electrophoresis frontal analysis, *Anal. Chem.* 88 (2016) 8050–8057. <https://doi.org/10.1021/acs.analchem.6b01430>.
- [30] C. Austin, S.N. Pettit, S.K. Magnolo, J. Sanvoisin, W. Chen, S.P. Wood, L.D. Freeman, R.J. Pengelly, D.E. Hughes, Fragment screening using capillary electrophoresis (CEfrag) for hit identification of heat shock protein 90 ATPase inhibitors, *J. Biomol. Screen.* 17 (2012) 868–876. <https://doi.org/10.1177/1087057112445785>.
- [31] M. Cheng, Z. Chen, Screening of tyrosinase inhibitors by capillary electrophoresis with immobilized enzyme microreactor and molecular docking, *Electrophoresis.* 38 (2017) 486–493. <https://doi.org/10.1002/elps.201600367>.
- [32] N.H.H. Heegaard, Affinity in Electrophoresis, *Electrophoresis.* 30 (2009) S229–S239. <https://doi.org/10.1002/elps.200900073>.
- [33] I.J. Colton, J.D. Carbeck, G.M. Whitesides, Affinity capillary electrophoresis: A physical-organic tool for studying interactions in biomolecular recognition, (1998) 367–382.
- [34] M. Ansorge, P. Dubský, K. Ušelová, Into the theory of the partial-filling affinity capillary electrophoresis and the determination of apparent stability constants of analyte-ligand complexes, *Electrophoresis.* 39 (2018) 742–751. <https://doi.org/10.1002/elps.201700385>.
- [35] A. Dementiev, A. Silva, C. Yee, Z. Li, M.T. Flavin, H. Sham, J.R. Partridge, Structures of human plasma β -factor XIIa cocrystallized with potent inhibitors, *Blood Adv.* 2 (2018) 549–558. <https://doi.org/10.1182/bloodadvances.2018016337>.
- [36] R.A. Copeland, Evaluation of enzyme inhibitors in drug discovery: a guide for medicinal chemists and pharmacologists, Second Ed., John Wiley & Sons, Hoboken, New Jersey, 2013.
- [37] P. Kuzmič, Program DYNAFIT for the analysis of enzyme kinetic data: Application to HIV proteinase, *Anal. Biochem.* 237 (1996) 260–273. <https://doi.org/10.1006/abio.1996.0238>.
- [38] A. Suratman, H. Wätzig, Reproducible protein analysis by CE using linear polyacrylamide-coated capillaries and hydrochloric acid rinsing, *Electrophoresis.* 28 (2007) 2324–2328. <https://doi.org/10.1002/elps.200700108>.
- [39] M. Nilsson, V. Harang, M. Bergström, S. Ohlson, R. Isaksson, G. Johansson, Determination of protein-ligand affinity constants from direct migration time in capillary electrophoresis, *Electrophoresis.* 25 (2004) 1829–1836. <https://doi.org/10.1002/elps.200405918>.
- [40] P. Dubský, M. Ördögová, M. Malý, M. Riesová, CEval: All-in-one software for data processing and statistical evaluations in affinity capillary electrophoresis, *J. Chromatogr. A.* 1445 (2016) 158–165. <https://doi.org/10.1016/j.chroma.2016.04.004>.
- [41] G. TANS, T. JANSSEN-CLAESSEN, J. ROSING, J.H. GRIFFIN, Studies on the effect of serine protease inhibitors on activated contact factors. Application in amidolytic assays for factor XIIa, plasma kallikrein and factor XIa, *Eur. J. Biochem.* 164 (1987) 637–642. <https://doi.org/10.1111/j.1432-1033.1987.tb11174.x>.
- [42] M.K. Ramjee, I.M.J. Henderson, S.B. McLoughlin, A. Padova, The Kinetic and Structural Characterization of the Reaction of Nafamostat with Bovine Pancreatic Trypsin, *Thromb. Res.* 98 (2000) 559–569. [https://doi.org/10.1016/S0049-3848\(00\)00206-1](https://doi.org/10.1016/S0049-3848(00)00206-1).
- [43] V. Baeriswyl, S. Calzavarini, S. Chen, A. Zorzi, L. Bologna, A. Angelillo-Scherrer, C. Heinis, A Synthetic Factor XIIa Inhibitor Blocks Selectively Intrinsic Coagulation Initiation, *ACS Chem. Biol.* 10 (2015) 1861–1870. <https://doi.org/10.1021/acschembio.5b00103>.
- [44] C. Davoine, C. Bouckaert, M. Fillet, L. Pochet, Factor XII/XIIa inhibitors: Their discovery, development, and potential indications, *Eur. J. Med. Chem.* 208 (2020)

112753. <https://doi.org/10.1016/j.ejmech.2020.112753>.
- [45] H. Stutz, Protein attachment onto silica surfaces - A survey of molecular fundamentals, resulting effects and novel preventive strategies in CE, *Electrophoresis*. 30 (2009) 2032–2061. <https://doi.org/10.1002/elps.200900015>.
- [46] M. Pathak, P. Wilmann, J. Awford, C. Li, B.K. Hamad, P.M. Fischer, I. Dreveny, L. V. Dekker, J. Emsley, Coagulation factor XII protease domain crystal structure, *J. Thromb. Haemost.* 13 (2015) 580–591. <https://doi.org/10.1111/jth.12849>.
- [47] D.K. Lloyd, H. Wätzig, Sodium dodecyl sulfate solution is an effective between-run rinse for capillary electrophoresis of samples in biological matrices, *J. Chromatogr. B Biomed. Sci. Appl.* 663 (1995) 400–405. [https://doi.org/10.1016/0378-4347\(94\)00440-G](https://doi.org/10.1016/0378-4347(94)00440-G).
- [48] M. Rabe, D. Verdes, S. Seeger, Understanding protein adsorption phenomena at solid surfaces, *Adv. Colloid Interface Sci.* 162 (2011) 87–106. <https://doi.org/10.1016/j.cis.2010.12.007>.
- [49] J. Wu, C. Zhao, W. Lin, R. Hu, Q. Wang, H. Chen, L. Li, S. Chen, J. Zheng, Binding characteristics between polyethylene glycol (PEG) and proteins in aqueous solution, *J. Mater. Chem. B*. 2 (2014) 2983–2992. <https://doi.org/10.1039/c4tb00253a>.
- [50] M. Jaroš, V. Hruška, M. Štědrý, I. Zusková, B. Gaš, Eigenmobilities in background electrolytes for capillary zone electrophoresis: IV. Computer program PeakMaster, *Electrophoresis*. 25 (2004) 3080–3085. <https://doi.org/10.1002/elps.200405982>.
- [51] T. Le Saux, A. Varenne, P. Gareil, Peak shape modeling by Haarhoff-Van der Linde function for the determination of correct migration times: A new insight into affinity capillary electrophoresis, *Electrophoresis*. 26 (2005) 3094–3104. <https://doi.org/10.1002/elps.200500029>.
- [52] M. Beneš, J. Svobodová, V. Hruška, M. Dvořák, I. Zusková, B. Gaš, A nonlinear electrophoretic model for PeakMaster: Part IV. Electromigration dispersion in systems that contain a neutral complex-forming agent and a fully charged analyte. Experimental verification, *J. Chromatogr. A*. 1267 (2012) 109–115. <https://doi.org/10.1016/j.chroma.2012.06.053>.
- [53] V. Hruška, J. Svobodová, M. Beneš, B. Gaš, A nonlinear electrophoretic model for PeakMaster: Part III. Electromigration dispersion in systems that contain a neutral complex-forming agent and a fully charged analyte. Theory, *J. Chromatogr. A*. 1267 (2012) 102–108. <https://doi.org/10.1016/j.chroma.2012.06.086>.
- [54] P. Dubský, M. Dvořák, L. Müllerová, B. Gaš, Determination of the correct migration time and other parameters of the Haarhoff-van der Linde function from the peak geometry characteristics, *Electrophoresis*. 36 (2015) 655–661. <https://doi.org/10.1002/elps.201400463>.
- [55] H. Bisswanger, *Enzyme kinetics: principles and methods*, Wiley-VCH Verlag GmbH & KGaA, Weinheim, 2008.
- [56] J.C. Hermann, Y. Chen, C. Wartchow, J. Menke, L. Gao, S.K. Gleason, N.E. Haynes, N. Scott, A. Petersen, S. Gabriel, B. Vu, K.M. George, A. Narayanan, S.H. Li, H. Qian, N. Beatini, L. Niu, Q.F. Gan, Metal impurities cause false positives in high-throughput screening campaigns, *ACS Med. Chem. Lett.* 4 (2013) 197–200. <https://doi.org/10.1021/ml3003296>.
- [57] M.M. Bernardo, D.E. Day, S.T. Olson, J.D. Shore, Surface-independent acceleration of factor XII activation by zinc ions. I. Kinetic characterization of the metal ion rate enhancement., *J. Biol. Chem.* 268 (1993) 12468–76.
- [58] A. Jadhav, R.S. Ferreira, C. Klumpp, B.T. Mott, C.P. Austin, J. Inglese, C.J. Thomas, D.J. Maloney, B.K. Shoichet, A. Simeonov, Quantitative analyses of aggregation, autofluorescence, and reactivity artifacts in a screen for inhibitors of a thiol protease, *J. Med. Chem.* 53 (2010) 37–51. <https://doi.org/10.1021/jm901070c>.

Legend to figures

Figure 1: Partial-filling ACE principle. At the beginning of the analysis (T_0), the analyte is at one end of the capillary and a part of capillary is filled with the target-spiked buffer. Upon voltage application (T_1), the analyte migrates through the target plug and a binding equilibrium occurs. At the end of the analysis (T_2), the analyte comes out of the target plug and reaches the detector in the target-free buffer. Therefore, the observed electrophoretic mobility of the analyte (μ_{obs}) at the end of the analysis is the results of the effective analyte mobility inside the plug ($\mu_{\text{A,eff}}$) and the analyte mobility (μ_{A}). The effective mobility inside the plug is a weighted average of the analyte mobility (μ_{A} – unbound fraction) and the complex mobility (μ_{Cpl} – bound fraction). The blue and orange parts of the capillary are, respectively, the analyte and target plugs.

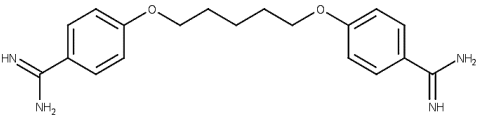
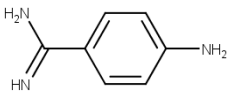
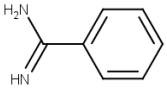
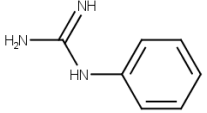
Figure 2. K_D determination for pentamidine-FXIIa interaction: (A) Electropherograms obtained with different FXIIa plug length and (B) Plot of the pentamidine migration times against the amount of injected β -FXIIa (in mol). The equation of the linear regression is $y = 1.87 \cdot 10^{12} x - 0.21$ and the R-square is 0.999. Based on the slope of this linear regression, K_D was determined at $6.30 \pm 0.07 \mu\text{M}$.

Figure 3. Screening results from pf-ACE (x value) in comparison with chromogenic FXIIa assay (y value). The lines tagged as threshold fixed the minimal signal needed to consider the compound as active.

Figure 4. IC_{50} of compound 3 (A) and PABZM (B) with and without 1 mM EDTA in the buffer. The IC_{50} of compound 3 without and with 1mM EDTA are, respectively, $713 \pm 23 \mu\text{M}$ (Hill slope = 1.06) and more than $3000 \mu\text{M}$. The IC_{50} of PABZM without and with 1mM EDTA are, respectively, $457 \pm 13 \mu\text{M}$ (Hill slope = 1.06) and $436 \pm 7 \mu\text{M}$ (Hill slope = 0.998).

Figure 5. Electropherograms of compound 3 (in black) and compound 3 spiked with 1.5 mM Zn^{2+} (in red). The insert compares the UV spectrum of compound 3 (in black) and Zn^{2+} -spiked compound 3 (in red) with those obtained with zinc (in blue) and nickel (in green).

Table 1. Reference compounds and their inhibition potency on FXIIa evaluated by the chromogenic assay. PABZM: p-aminobenzamidine. BZM: benzamidine. PhGu: phenylguanidine. IC₅₀: inhibitory concentration at 50%. K_i: inhibition constant. S_D: standard deviation. NT: not tested.

Compounds	Structure	Bound fraction ± S _D (%)	K _D ± S _D (μM)	Inhibition at 1mM ± S _D (%)	IC ₅₀ ± S _D (μM)	K _i ± S _D (μM)
<i>Pentamidine</i>		66.3 (± 0.2)	6.30 (± 0.07)	98 (± 7)	31.9 (± 0.7)	12.4 (± 0.1)
<i>PABZM</i>		8.0 (± 0.1)	149 (± 14)	69 (± 7)	457 (± 13)	163.2 (± 0.5)
<i>BZM</i>		1.6 (± 0.3)	NT	34.4 (± 0.8)	2377 (± 84)	NT ^a
<i>PhGu</i>		-0.34 (± 0.3)	NT	3.4 (± 0.1)	16900 (± 667)	NT

^a Reported by Tans et al.[41] at 1.12 mM (pH 7.2)

Table 2. Investigations of the method precision. (A) Sample injection procedure ($n = 3$; β -FXIIa exposition = 0; $L_{tot} = 30$ cm, $L_{eff} = 21.5$ cm; $V = 4$ kV). **(B) Rinse protocol. (C) Precision obtained during screening.** AUC: area under the curve. BGE: background electrolytes. M_t : migration time. RSD: relative standard deviation. S_D : standard deviation. μ : electrophoretic mobility.

A

Sample injection procedure	Sample solvent	M_t (min)		AUC	
		Mean $\pm S_D$	RSD %	Mean $\pm S_D$	RSD %
50 mbar sample for 2s	BGE	7.9 \pm 0.03	0.3	10.9 \pm 0.21	1.9
	Diluted BGE [§]	7.8 \pm 0.02	0.2	10.7 \pm 0.61	5.7
20 mbar sample for 5s	BGE	7.8 \pm 0.02	0.2	10.9 \pm 0.36	3.3
	Diluted BGE [§]	7.8 \pm 0.02	0.3	10.4 \pm 0.05	0.5

[§]Diluted BGE corresponds to the BGE 10-fold diluted with water.

B

Rinse protocol	Number of runs (n)	Number of β -FXIIa exposition	M_t (min)		μ ($10^{-9} \cdot m^2 \cdot V^{-1} \cdot s^{-1}$)	
			Mean $\pm S_D$	RSD %	Mean $\pm S_D$	RSD %
None ^a	7	3	10.0 \pm 0.31	3.1	34.8 \pm 1.1	3.0
SDS ^b	7	3	10.3 \pm 0.68	6.6	33.7 \pm 2.2	6.7
2M HCl ^c	56	21	11.3 \pm 0.21	1.9	34.0 \pm 0.63	1.8

^a ($L_{tot} = 30$ cm, $L_{eff} = 21.5$ cm; $V = 3.1$ kV)

^b Rinse protocol described by Lloyd et al.[47] applied after each β -FXII exposition ($L_{tot} = 30$ cm, $L_{eff} = 21.5$ cm; $V = 3.1$ kV)

^c Rinse protocol described by Suratman et al.[38] applied after every 3 β -FXIIa exposition ($L_{tot} = 33$ cm, $L_{eff} = 24.5$ cm; $V = 3.5$ kV)

C

Quality controls during screening		M_t (min)		μ ($10^{-9} \cdot m^2 \cdot V^{-1} \cdot s^{-1}$)	
		Mean $\pm S_D$	RSD %	Mean $\pm S_D$	RSD %
Intra-day (n = 5)	Highest RSD	13.2 \pm 0.15	1.1	34.1 \pm 0.38	1.1
Inter-day (n = 121)		12.9 \pm 0.21	1.6	34.8 \pm 0.56	1.6

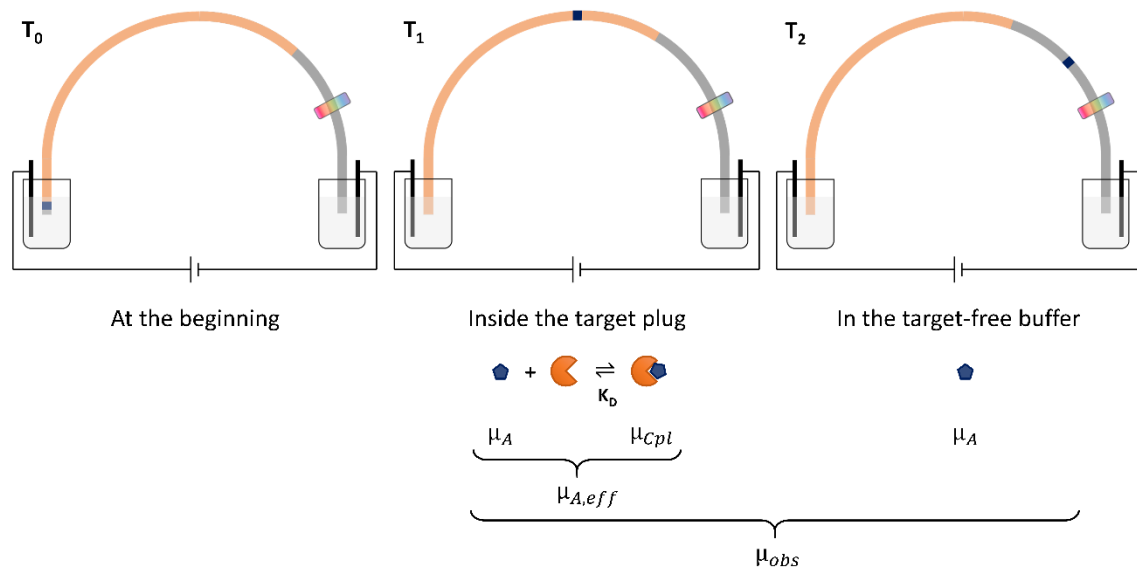


Figure 2: Partial-filling ACE principle. At the beginning of the analysis (T_0), the analyte is at one end of the capillary and a part of capillary is filled with the target-spiked buffer. Upon voltage application (T_1), the analyte migrates through the target plug and a binding equilibrium occurs. At the end of the analysis (T_2), the analyte comes out of the target plug and reaches the detector in the target-free buffer. Therefore, the observed electrophoretic mobility of the analyte (μ_{obs}) at the end of the analysis is the results of the effective analyte mobility inside the plug ($\mu_{A,eff}$) and the analyte mobility (μ_A). The effective mobility inside the plug is a weighted average of the analyte mobility (μ_A – unbound fraction) and the complex mobility (μ_{Cpl} – bound fraction). The blue and orange parts of the capillary are, respectively, the analyte and target plugs.

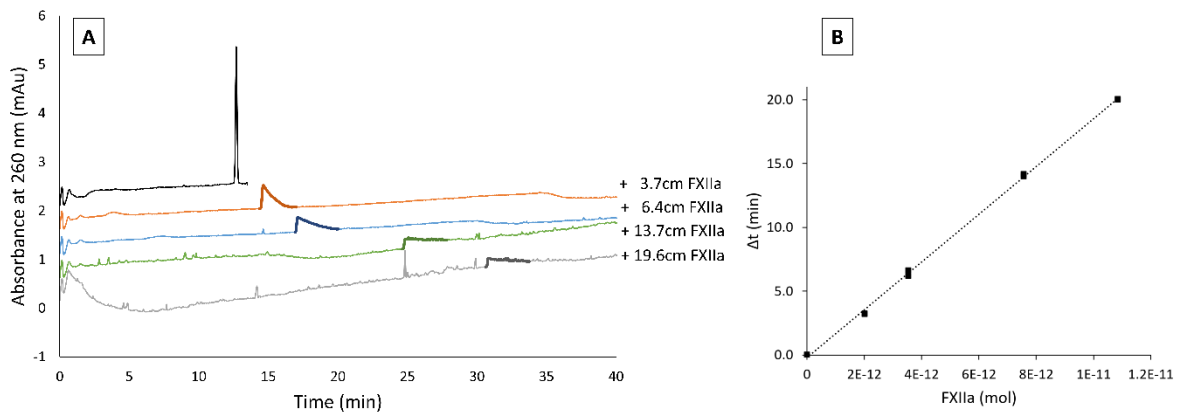


Figure 2. K_D determination for pentamidine-FXIIa interaction: (A) Electropherograms obtained with different FXIIa plug length and (B) Plot of the pentamidine migration times against the amount of injected β -FXIIa (in mol). The equation of the linear regression is $y = 1.87 \cdot 10^{12} x - 0.21$ and the R-square is 0.999. Based on the slope of this linear regression, K_D was determined at $6.30 \pm 0.07 \mu\text{M}$.

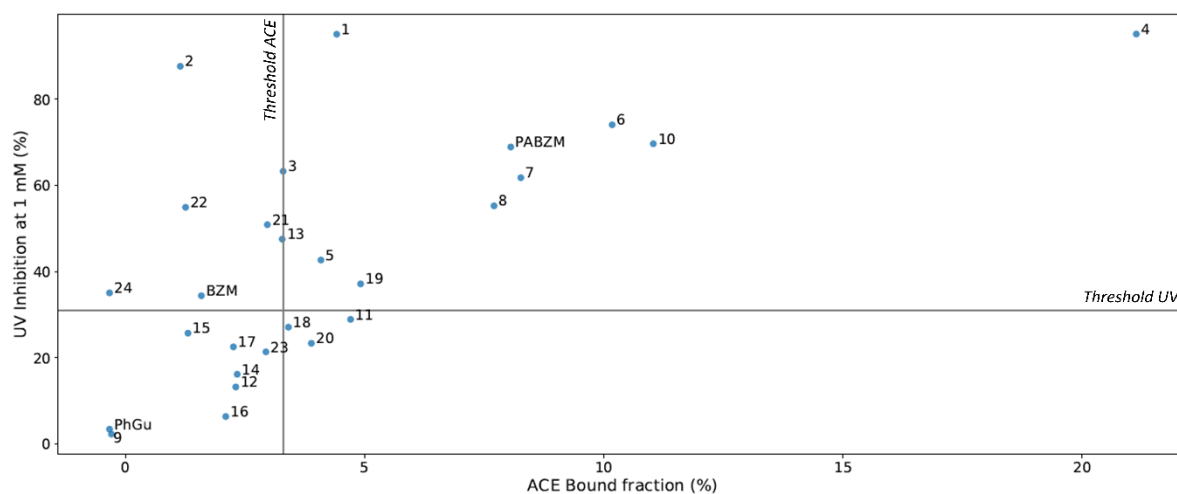


Figure 3. Screening results from pf-ACE (x value) in comparison with chromogenic FXIIa assay (y value). The lines tagged as threshold fixed the minimal signal needed to consider the compound as active.

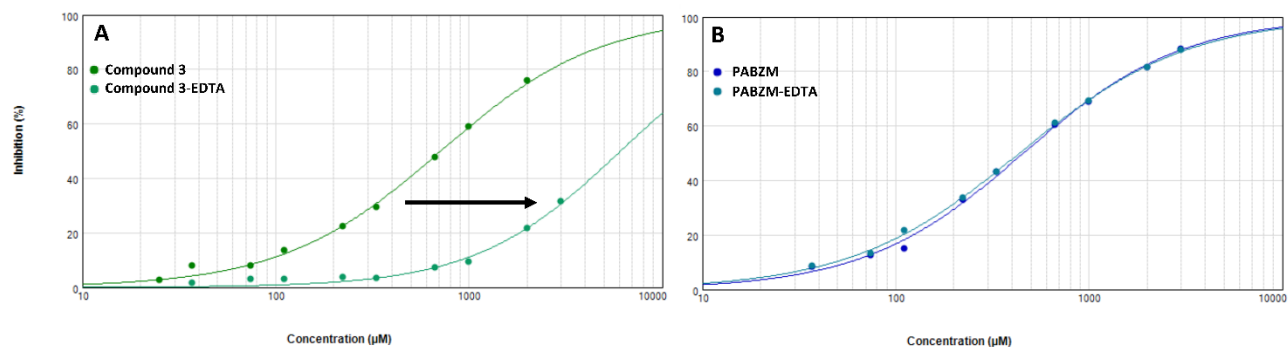


Figure 4. IC₅₀ of compound 3 (A) and PABZM (B) with and without 1 mM EDTA in the buffer. The IC₅₀ of compound 3 without and with 1mM EDTA are, respectively, $713 \pm 23 \mu\text{M}$ (Hill slope = 1.06) and more than $3000 \mu\text{M}$. The IC₅₀ of PABZM without and with 1mM EDTA are, respectively, $457 \pm 13 \mu\text{M}$ (Hill slope = 1.06) and $436 \pm 7 \mu\text{M}$ (Hill slope = 0.998).

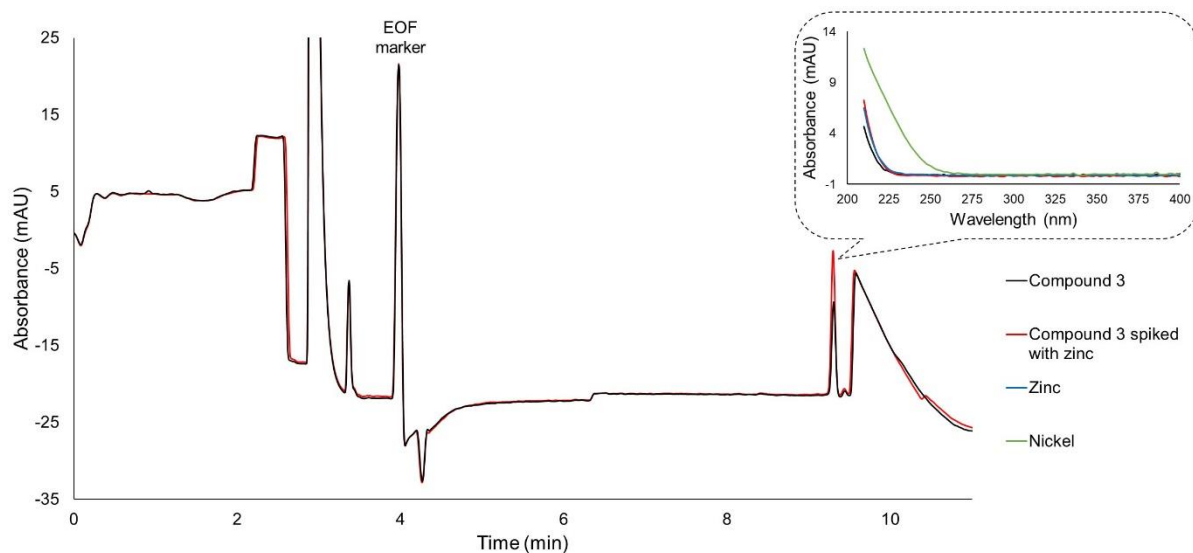


Figure 5. Electropherograms of compound 3 (in black) and compound 3 spiked with 1.5 mM Zn²⁺ (in red). The insert compares the UV spectrum of compound 3 (in black) and Zn²⁺-spiked compound 3 (in red) with those obtained with zinc (in blue) and nickel (in green).